Journal of Materials Chemistry C

Two-dimensional square-pyramidal VO2 with tunable electronic properties

Journal:	*Journal of Materials Chemistry C*
Manuscript ID:	TC-ART-12-2014-002938.R1
Article Type:	Paper
Date Submitted by the Author:	16-Jan-2015

Complete List of Authors:	Tang, Zhen-Kun; Beijing Computational Science Research Center, ; Hengyang Normal University, Departments of Physics and Electronics Li, Xibo; Beijing Computational Science Research Center, Zhang, Deng-Yu; Hengyang Normal University, Departments of Physics and Electronics Zhang, Yanning; Chengdu Green Energy and Green Manufacturing Technology R&D Center, ; Beijing Computational Science Research Center, Liu, Li-Min; Beijing Computational Science Research Center,

Two-dimensional square-pyramidal VO_2 with tunable electronic properties

Zhen-Kun Tang[1,2], Xi-Bo Li[1], Deng-Yu Zhang[2], Yan-Ning Zhang[1,3], Li-Min Liu[1]*

[1]Beijing Computational Science Research Center, Beijing 100084, China
[2]Departments of Physics and Electronics, Hengyang Normal University, Hengyang 421008, China
[3]Chengdu Green Energy and Green Manufacturing Technology R&D Center, Chengdu, Sichuan, 610207, China

Email: limin.liu@csrc.ac.cn

Abstract: In order to design the high-performance spintronics, it is rather critical to develop new materials, which can easily regulate the magnetism of nanostructures. In this work, the electronic properties of two dimensional (2D) square-pyramidal vanadium dioxide (S-VO_2) are explored based on first-principle calculations. The results reveal that the monolayer S-VO_2 is an ideal flexible platform to manipulate the magnetic properties by either biaxial compressive strain or surface modification. Although the ground state of the pristine S-VO_2 is a direct semiconductor with antiferromagnetic (AFM) coupling between two nearest V atoms, the monolayer S-VO_2 becomes ferromagnetic (FM) under a biaxial compressive strain. Furthermore, the monolayer S-VO_2 can be tuned from nonmagnetic semiconductor to magnetic semiconductor and even to half-metal through surface modification. The tunable magnetic properties of the monolayer S-VO_2 make it promising candidate for applications in spin-devices.

1. Introduction

Two-dimension (2D) layered materials[1-6] have received tremendous attentions in the past ten years due to the unusual physical properties from their three-dimension (3D) counterparts. In particular, novel 2D materials with the intrinsic magnetism are crucial for the relatively novel field of spintronics[7]. Much of these technological achievements stem from the unique physical properties of the 2D or quasi-2D magnetic systems. For example, quasi-2D magnetic multilayers demonstrate the extraordinary properties of oscillating exchange coupling[8] and giant magnetoresistance[9] (GMR).

Recent theory studies demonstrate that some of monolayer transition-metal dichalcogenides, such as VX_2[10, 11] (X=S, Se) and MnX_2[12, 13] (X=O, S, Se), own intrinsic ferromagnetism in the pristine layered structures. Moreover, the room temperature ferromagnetism of the ultrathin VS_2 nanosheets has been detected by experimental measurements[14]. In general, most of the layered MX_2 are thermodynamically stable in the conventional trigonal (T) and/or hexagonal (H) structures[15], while some MX_2 compounds are stable in multiple forms of crystalline structures[16].

Vanadium dioxide (VO_2) becomes attractive in both industrial and scientific areas because of its reversible metal–insulator transition (MIT) between monoclinic VO_2 (M) and rutile (R) VO_2 phases[17, 18], associated with the benefits of huge temperature-induced resistivity changes[19]. In addition, there are other five VO_2 phases, such as triclinic VO_2, tetragonal VO_2, monoclinic VO_2, paramontroseite VO_2, and body centered-cubic VO_2 structure[20, 21]. The polymorphic feature of VO_2 offers great chances to find some possible novel 2D structures with the versatile electronic structures. The thermodynamic stabilities of the conventional trigonal VO_2 (T-VO_2) and hexagonal VO_2 (H-VO_2) monolayers were examined using first-principle calculations and finite-temperature ab initio molecular dynamics calculations[15]. The results showed that the layered H-VO_2 could be stable only at small size due to the instability occurring in long-wavelength acoustical mode. Another possible square-pyramidal monolayer VO_2 (S-VO_2) structure has been experimentally fabricated through the dehydration and electrochemical delithiation of $Li_{0.6}V_{2-\delta}O_{4-\delta}H_2O$[22, 23]. The pyramidal monolayer S-VO_2 are arranged in the up-down-up-down chess-board like manner, which is closely related to the layered V_2O_5[24]. While there is still no related theoretical work on the monolayer S-VO_2.

It is well known that theoretical calculation plays an extremely important role in the forecasting of novel materials, and many novel 2D crystalline phases have been suggested in first-principles calculations[25-31]. For example, Li *et al*. put forward the novel 2D network of SiC_4 by first-principles calculations[25]. Zhang *et al*. proposed 2D tetragonal TiC monolayer with an indirect band gap[26]. Then, the properties of quasi-2D Ti_mC_n[27] and Ti_mN_n[28] nanomaterials have been studied in the framework of the density functional theory. Besides, 2D tetragonal monolayer MgO (100)[29], tetragonal monolayer AlX (X=P, As)[30] and monolayer B_2C[31] are also predicted by theoretical calculations.

In this work, first-principles calculations were carried out to systematically

examine the stability, electronic structure, and magnetic properties of the monolayer S-VO_2. The monolayer S-VO_2 is thermodynamically stable, and it is a direct band gap semiconductor. The ground state of the monolayer S-VO_2 is antiferromagnetic, and the magnetic moments are mainly contributed by d_{xy} orbitals of V atoms. Interestingly, the magnetism of the monolayer S-VO_2 can transform into ferromagnetic under a biaxial compressive strain, and the magnetism can be further modulated by surface modification. The half-hydrogenated and half-fluorinated monolayer S-VO_2 exhibits unusual half-metal (HM) properties. The versatile electronic and magnetic properties of the monolayer S-VO_2 open a new door to explore the spintronics in pristine 2D material.

2. Computational Method

The first-principles structure and energy calculations are performed using the Vienna Ab Initio Simulation Package (VASP)[25, 26]. Projector augmented-wave (PAW) pseudopotentials[27] were used to account electron-ion interactions. The generalized gradient approximation (GGA) with the PBE functional[28] was used to treat the exchange-correlation interaction between electrons. A vacuum region larger than 15 Å perpendicular to the sheets (along the **c** axis) is applied to avoid the interaction between layers caused by the periodic boundary condition. In our calculation, a kinetic-energy cutoff for plane-wave expansion is set to 500 eV. All the atoms in the unit cell are fully relaxed until the force on each atom is less than 0.005 eV/Å. Electronic energy minimization was performed with a tolerance of 10^{-6} eV. The Brillouin-zone (BZ) sampling is carried out with a 21×21×1 Monkhorst-Pack grid for the 2D sheets. In order to avoid the shortcoming of conventional PBE calculation, the hybrid Heyd-Scuseria-Ernzerhof functional (HSE06)[29, 30] calculations are used to calculate the accurate electronic structure and band gap based on PBE geometries.

Phonon dispersion spectrum analysis is an important way to examine the stability of a specific system. If any imaginary frequency exists in the phonon spectrum, the system is dynamic unstable. In this work, the phonon spectrum is calculated with the PHONOPY package[31], which uses the Parlinski–Li–Kawazoe approach[32]. For this calculation, a large 4×4×1 supercell is used. In order to determine the force constants, three non-symmetry equivalent displacements are applied to the structure.

3. Results and Discussion

3.1 The structure and stability of the 2D VO_2

As mentioned in the introduction, VO_2 is polymorphic, and the typical structures are S-VO_2 and H-VO_2. In this work, the structures and stabilities of the monolayer S-VO_2 and H-VO_2 are considered. The corresponding monolayer structures of S-VO_2 and H-VO_2 are shown in Figure 1 (a) and Figure 1 (b), respectively. The S-VO_2 structure is P4/NMM-6M (D_{4h}) point group symmetry, with V atom bonding to five neighboring O atoms; and the H-VO_2 structure belongs to P-6M2(D_{3h}) point group symmetry, with V atom bonding to six neighboring O atoms. The optimized lattice constants of the monolayer S-VO_2 and H-VO_2 with PBE functional are 3.745 and 2.747 Å, respectively. The lattice constant of the monolayer H-VO_2 agrees well with

the previous calculated value of 2.70 Å[15].

In order to know the relative stability between these two structures, the formation energy, E_f, are calculated, which stands for the released energy when compounds form from the corresponding elements. The formation energy of the monolayer VO_2 is defined as follows,[11]

$$E_f = E_{bulk}(V) + E_{gas}(O_2) - E(VO_2)$$

where $E_{bulk}(V)$, $E_{gas}(O_2)$ and $E(VO_2)$ represent the total energies of the equilibrium bulk V, oxygen molecule and monolayer VO_2, respectively. The calculated formation energies of the monolayer VO_2 are 7.379 and 7.108 eV for S-VO_2 and H-VO_2, respectively. The larger formation energy shows the higher stability relative to free V and O atoms. It should be pointed out that the formation energy of the monolayer S-VO_2 is about 0.271 eV larger than that of monolayer H-VO_2, indicating that the monolayer S-VO_2 is more stable.

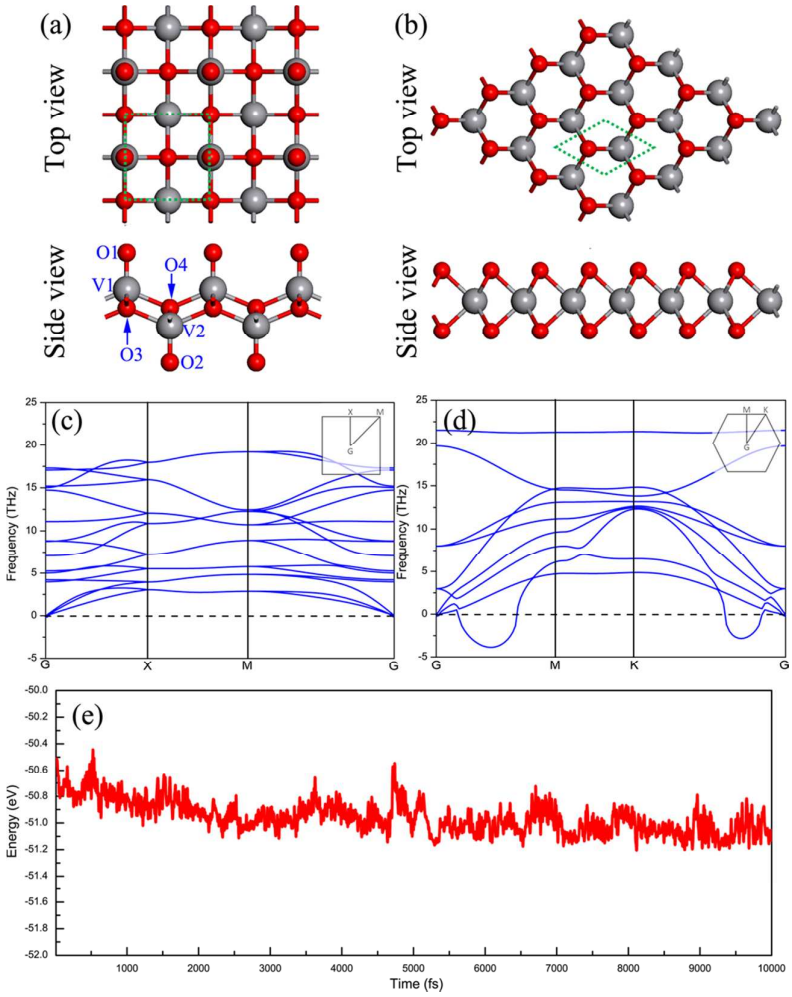

Figure 1 *The relaxed atomic structures of the monolayers (a) S-VO_2 and (b) H-VO_2. Phonon dispersions are along the high-symmetry directions in the BZ of monolayer S-VO_2 (c) and H-VO_2 (d), respectively. (e)The potential energy changes as a function of the simulation time during first principle molecular dynamic simulations for S-VO_2. The red and grey balls represent O atoms and V atoms, respectively. The different atoms of the S-VO_2 unit cell are labeled as V_1, V_2, O_1, O_2, O_3,*

and O_4, respectively. The detailed magnetic moments of these atoms are given in Table 1.

To further check their thermodynamically stabilities, frequencies of the monolayer S-VO_2 and H-VO_2 were further calculated for all k points in the BZ. The phonon dispersions along the high-symmetry directions in the BZ of the monolayer S-VO_2 and H-VO_2 are presented in Figure 1 (c) and Figure 1 (d), respectively. For the monolayer S-VO_2, the frequencies of all phonon modes in the BZ are positive, which shows again the high stability of this 2D layered structure. However, the imaginary frequencies of the monolayer H-VO_2 appears. Recently, Ataca et al. also examined the stability of the monolayer H-VO_2 by first-principle calculations, and the same imaginary frequencies are reported[15]. Therefore, the monolayer H-VO_2 should be thermodynamically unstable at room temperature. Besides, first-principle molecular dynamics (FPMD) simulations are also performed to confirm the thermal stability of the monolayer S-VO_2. As shown in Figure 1 (e), no energy jump occurs for the monolayer S-VO_2 during the whole molecular dynamic simulation of 10 ps at T = 300 K, and the monolayer S-VO_2 remains intact. Thus, S-VO_2 sheet are thermodynamically stable at the room temperature. In the following, only the stable monolayer S-VO_2 is further considered.

3.2 The electronic structure and magnetic coupling of the monolayer S-VO_2

As mentioned in the introduction, Chirayil et al. has experimentally synthesized a new form of S-VO_2 using the hydrothermal reaction of vanadium pentoxide and lithium hydroxide in the presence of an organic templating cation[22, 23]. The hydrated lithium S-VO_2 formed has the simplest layered structure, containing only square pyramids whose apices alternate up and down in the layer. However, the potential electronic properties of such monolayer S-VO_2 have not been examined in both experiment and theory. Considering the partially filled 3d shells of the vanadium (V) atom, the monolayer S-VO_2 may exhibit special electronic properties in the spin polarization and magnetic coupling.

The calculated results with PBE show that the most stable state of the monolayer S-VO_2 is antiferromagnetic (AFM), which is about 63 and 537 meV per cell lower than the ferromagnetic (FM) and nonmagnetic (NM) states, respectively. The calculated band structures and density of states (DOS) of the AFM monolayer S-VO_2 are shown in Figure 2 (a). The band structures with PBE show that the pristine monolayer S-VO_2 is a semiconductor with a direct band gap of 1.25 eV at the M point. The calculated spin density of the monolayer S-VO_2 (see Figure 2 (c)) clearly show that the spin density of AFM is mainly localized on the V atom with ~1 μ_B per V atom. However, the pristine monolayer S-VO_2 does not exhibit macro magnetic properties because of the AFM coupling.

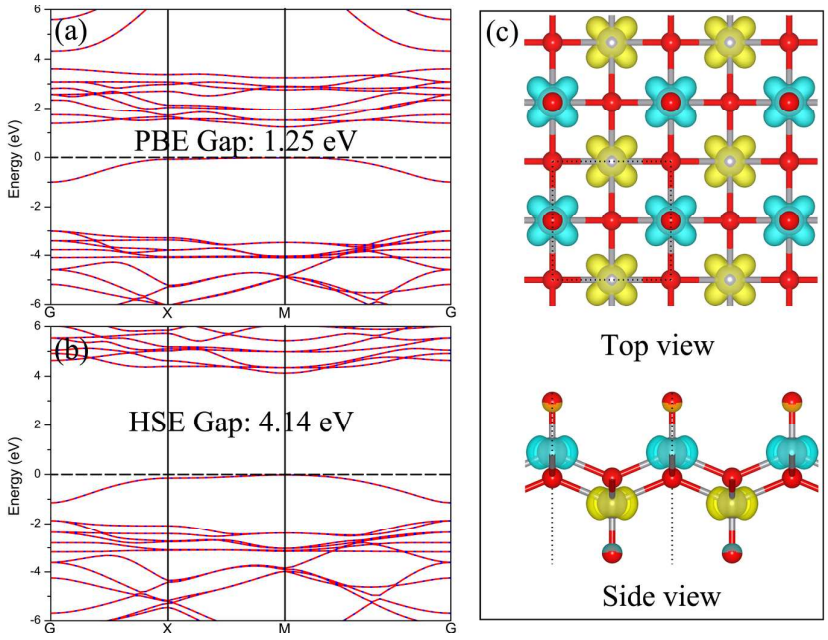

Figure 2 *Calculated band structures for the AFM monolayer S-VO_2 by (a) PBE and (b) hybrid HSE06, respectively. The red solid lines and blue dashed lines in the band structures images represent the spin up bands and spin down bands, respectively. (c) The spin density distributions of the monolayer S-VO_2. The red and grey balls represent O and V atoms, respectively. The yellow and green isosurfaces correspond to the densities of spin up and spin down, respectively.*

It is well known that the conventional PBE functional usually underestimates the band gap of semiconductors because of the self-interaction error[33, 34]. The hybrid functional usually gives the more reasonable electronic structure, while it is rather expensive to optimize the geometries to calculate the electronic structure. Thus, in this work, the energy differences between AFM and FM coupling of the monolayer S-VO_2 are mainly calculated with PBE, while the electronic structures are analyzed with HSE06 based on the PBE geometries. In order to check the reliability of such approach, another calculation on the pristine monolayer S-VO_2 with HSE06 is also carried out. The geometry is fully optimized with HSE06, and then the other properties are further calculated with HSE06. Firstly, the optimized lattice constant of the stress-free S-VO_2 is 3.71 Å with HSE06, which is close to the value of 3.74 Å with PBE. Secondly, the energy differences between AFM and FM coupling of the stress-free S-VO_2 is -27 meV with HSE06 based on the geometries optimized with HSE06, which is close to the value of -62 meV with PBE. Thirdly, the electronic structures calculated with HSE06 based on both PBE and HSE06 geometries show quite similar results. The band gap of the stress-free S-VO_2 based on the hybrid HSE06 geometry is 4.15 eV, which is quite close to the corresponding ones, 4.14 eV (see Figure 2(b)), calculated with HSE06 based on the PBE geometries. Such results clearly suggest that the PBE functional can describe well the structure and energy of the monolayer S-VO_2. In the following, we mainly discuss the structure and energy

calculated with PBE, and the electronic properties calculated with HSE06 based on PBE geometries except we note.

To obtain deeper insight into the electronic structure of the monolayer S-VO_2, the orbital-projected DOS is analyzed. As shown in Figure 3 (a), the d_{xy} orbital of V atom (V-d_{xy}) is obviously lower energetically than the other V-3d orbitals, locating just below the Fermi level (E_F). In addition, there is no any overlap between V-d_{xy} and O-2p states. The main reason is that V atom stays in the square-pyramidal O ligand field, which has no O ligand atom in the x-y plane, as showed in Figure 3 (b). According to the orbital-projected DOS of V and O atom, the schematic coupling diagram of the energy levels is plotted in Figure 3 (c). The coupling between different energy levels is analyzed by the reciprocal repulsion model[35], which is helpful to further understand the origin of magnetism in the monolayer S-VO_2.

As for the neutral monolayer S-VO_2, most of V-3d sub-orbitals are pushed to a higher energy level by O-2p orbital. However, the V-d_{xy} orbital does not change due to no interaction between V-d_{xy} and O-2p orbitals around the Fermi level. It is well-known that V atom consists of five outer electrons as $3d^34s^2$, and each V atom keeps an extra electron after its combination with two O atoms. The only extra electron occupies the V-d_{xy} orbital, whereas the other four V-3d orbitals are empty. Thus, the magnetic moment of the monolayer S-VO_2 comes from V-d_{xy} orbital. This explains why the shape of the spin density is a typical d_{xy} orbital (see Figure 2 (c)). The coupling between the different energy levels results in the splitting of V-3d orbitals and the shape of spin density distribution of the monolayer S-VO_2.

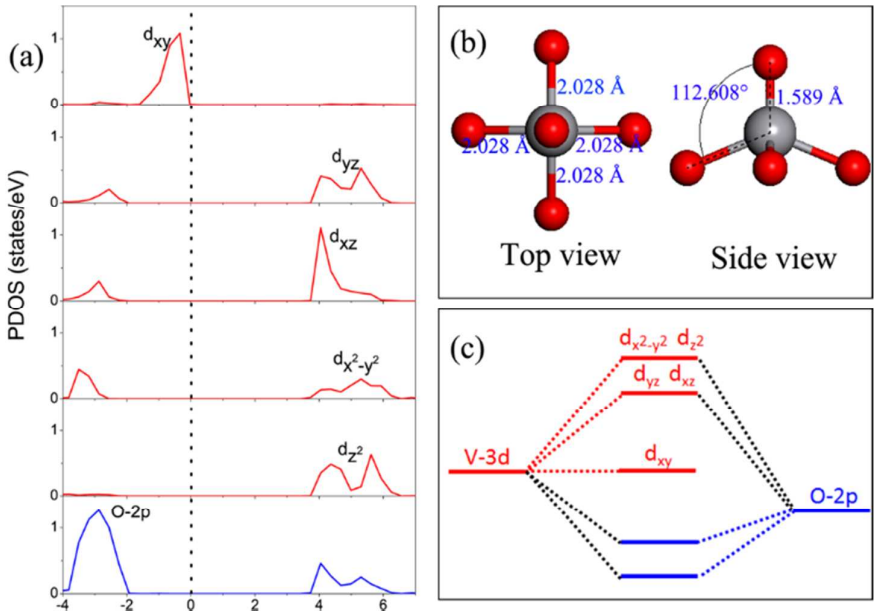

Figure 3 *(a) The orbital-projected DOS of V-3d and O-2p states in the monolayer S-VO_2. (b) The square-pyramidal V-O ligand field and the corresponding V-O bond length and O-V-O bond angle. (c) Schematic coupling diagram of the energy levels in monolayer S-VO_2.*

3.3 Compressive strain switch on ferromagnetism of the monolayer S-VO_2

Strain is widely used approach to induce and engineer the magnetic properties of

MX_2 layered materials[10, 36, 37]. Thus, it is desirable to know whether the strain can effectively tune magnetic behavior of the monolayer S-VO_2. Here, we investigate the strain effect on the magnetic properties of the monolayer S-VO_2 by varying the biaxial strain from -10% to 10%. Figure 4 (a) shows the variation of the energy difference between AFM and FM state (E_{afm}-E_{fm}) as a function of applied strain, and the positive (negative) values represent that the FM (AFM) is the ground state of the monolayer S-VO_2. Interestingly, E_{afm}-E_{fm} changes from negative to positive under a compressive strain of about 7%. When a compressive strain of up to 8% applies, a typical FM coupling occurs with 2 μ_B magnetic moment per unit cell.

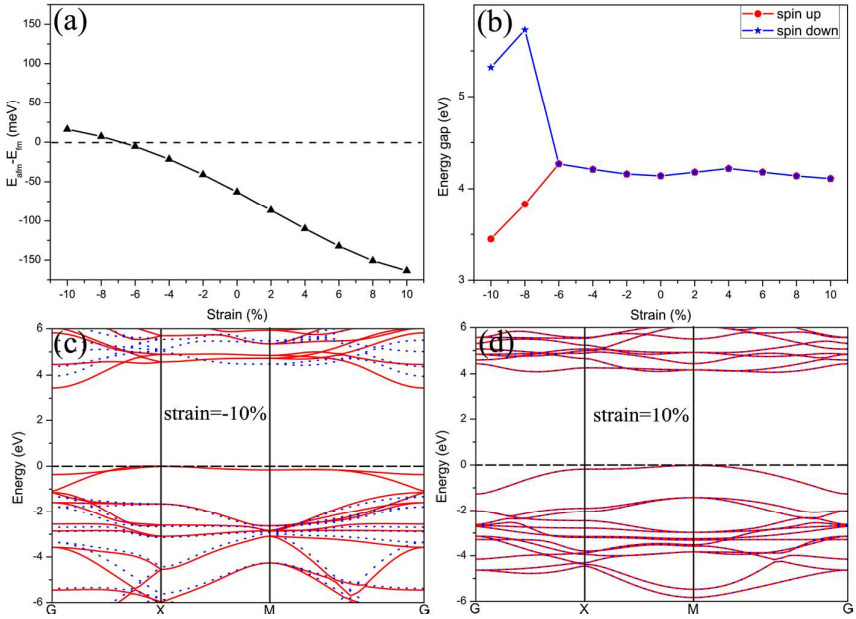

Figure 4 *(a) The E_{afm}-E_{fm} variation of the monolayer S-VO_2 with PBE under strains. (b) The* spin-up (*red dots*) and spin-down (*blue stars*) *band gaps of the monolayer S-VO_2 with strain. The band structures of the monolayer S-VO_2 under biaxial compressive strain of -10% (c) and biaxial tensile strain of 10% (d). All the band structures are calculated with HSE06. The red solid lines and blue dashed lines represent the spin up bands and spin down bands, respectively.*

The spin polarized band structures under 10% compressive strain and 10% tensile strain are shown in Figure 4 (c) and 4 (d), respectively. With a 10% compression, the monolayer S-VO_2 becomes an indirect semincondutor, and the band gap decreases to 3.45 eV. Moreover, both the conduction band minimum (CBM) and the valence band maximum (VBM) behave as spin up. Thus, the macro magnetism should exist in the compressed monolayer S-VO_2. The band structure under 10% tensile strain (see Figure 4 (d)) exhibit a qualitatively similar behavior with the non-pressure band structure in Figure 2 (b), indicating that the tensile strain has little effect on the band structure of the monolayer S-VO_2. The evolutions of spin-up and spin-down band gaps under strains are shown in Figure 4 (b). As for the AFM state, the band gap does not change significantly under either compressive or tensile strains. In contrast, the spin-up band gap in FM state dramatically drops under compressive strains, implying a decreased band gap in the monolayer S-VO_2.

As mentioned above, the energy differences between antiferromagnetic (AFM) and ferromagnetic (FM) coupling of the monolayer S-VO_2 are mainly calculated with PBE, while the electronic structures are analyzed with HSE06 based on the PBE geometries. In order to check the reliability of such approach on the strain monolayer S-VO_2, the hybrid HSE06 functional are employed to examine whether the structure relaxations affect the electronic structure. The typical system of the monolayer S-VO_2 under a compressive strain of 10% is used. The geometries are firstly optimized with HSE06, and then the other properties are further calculated. Firstly, the energy differences between AFM and FM coupling of the compressived S-VO_2 is 10 meV with HSE06 (the geometries are also fully optimized with HSE06), which is quite close to the value of 16 meV with PBE. Secondly, the electronic structures calculated with HSE06 based on both PBE and HSE06 geometries are quite similar results. The up and down band gaps of the compressived S-VO_2 based on the hybrid HSE06 geometries are 3.57 eV and 5.33 eV, respectively. The results are quite close to the corresponding ones, 3.45 eV and 5.32 eV, calculated with HSE06 based on the PBE geometries. Such tests further suggest that the approach used above is reliable to examine the electronic properties of the monolayer S-VO_2.

To further understand the distributions of the magnetic moments in the monolayer S-VO_2, we show the magnetic moment of each atom in Table 1. The different atoms are labeled in Figure 1 (a). The total magnetic moment of the monolayer S-VO_2 is 2 and 0 μ_B per cell in FM and AFM coupling, respectively. Both of the compressive strain and tensile strain do not significantly change the magnitude of the magnetic moment on single atom. The magnetic moments are localized mainly on the V atom with about 1 μ_B per atom, and the induced magnetic moments on top O atoms (O1 and O2) are bigger than those on in-plane O atoms (O3 and O4). The tunable magnetism of the monolayer S-VO_2, by using biaxial compressive strain, enables it to apply in spintronics devices. Given the recent progress in achieving the desired strain on 2D graphene[38, 39], the monolayer S-VO_2 are suitable for experimental verification and implementation.

Table 1 *Magnetic moment of VO_2 structures under the different strains (The unit is μ_B). The corresponding atoms are labelled in Figure 1.*

Strain (%)	Total	V_1	V_2	O1	O2	O3	O4
-10	2.000	1.072	1.072	-0.133	-0.133	0.002	0.002
-8	2.000	1.076	1.076	-0.137	-0.137	0.004	0.004
-6	0.000	-1.052	1.052	0.148	-0.148	0.018	-0.018
-4	0.000	-1.058	1.058	0.150	-0.150	0.019	-0.019
-2	0.000	-1.063	1.063	0.153	-0.153	0.020	-0.020
0	0.000	-1.069	1.069	0.157	-0.157	0.021	-0.021
2	0.000	-1.075	1.075	0.153	-0.153	0.020	-0.020
4	0.000	-1.081	1.081	0.165	-0.165	0.022	-0.022
6	0.000	-1.087	1.087	0.170	-0.170	0.022	-0.022
8	0.000	-1.094	1.094	0.174	-0.174	0.023	-0.023
10	0.000	-1.101	1.101	0.179	-0.179	0.023	-0.023

3.4 Modulating the magnetic properties of the monolayer S-VO_2 by surface modification

It is well known that the electronic and magnetic properties of many 2D materials, such as graphene, can be tuned by surface modification[40-42]. Now the following questions arise: since a monolayer S-VO_2 is semiconductor with AFM coupling, is the hydrogenated monolayer S-VO_2 metallic or semiconducting? Is it FM or AFM ground state?

Table 2 *The band gap, magnetic coupling and magnetic moment distribution of S-VO_2 structures with different surface modifications: fully hydrogenated monolayer S-VO_2 (S-VO_2-2H), fully-fluorinated monolayer S-VO_2 (S-VO_2-2F) and half-hydrogenated and half-fluorinated monolayer S-VO_2 (S-VO_2-HF).*

Structure	E_{afm}-E_{fm} (meV)	$E_{gap\text{-}up}$ (eV)	$E_{gap\text{-}down}$ (eV)	M_{V1} (μ_B)	M_{V2} (μ_B)	M_{total} (μ_B)
S-VO_2-2H	9	1.37	6.08	1.843	1.843	3.986
S-VO_2-2F	-146	3.39	3.39	- 0.384	0.384	0.000
S-VO_2-HF	233	/	5.04	1.728	0.905	2.718

To answer these questions, the relative stability between AFM and FM is explored for fully hydrogenated monolayer S-VO_2 (S-VO_2-2H). The optimized bond lengths of V–O (top), V–O (side) and O–H are 1.801, 2.014 and 0.960 Å, respectively. The detailed band gap and magnetic moments of the monolayer S-VO_2-2H are listed in Table 2. The calculated E_{afm}-E_{fm} of the fully-hydrogenated monolayer S-VO_2 suggests that the monolayer S-VO_2-2H prefers FM coupling, along with about 4 μ_B per unit cell.

As shown in Figure 5, the monolayer S-VO_2-2H is an indirect band gap semiconductor with a small band gap of 1.37 eV. Both of the valence band and the conductance band are contributed by spin up states. The VBM locates at the G point, while the CBM is near the X point. The DOS exhibits that the magnetic moments mainly come from the V atom. The magnetic moment of a single V atom in S-VO_2-2H is noticeably larger than the one in pristine monolayer S-VO_2 due to the electron donations from H atom. More importantly, the FM coupling between the V atoms can be obtained by hydrogen modification, which can be concluded as carries-controlled ferromagnetism[43, 44].

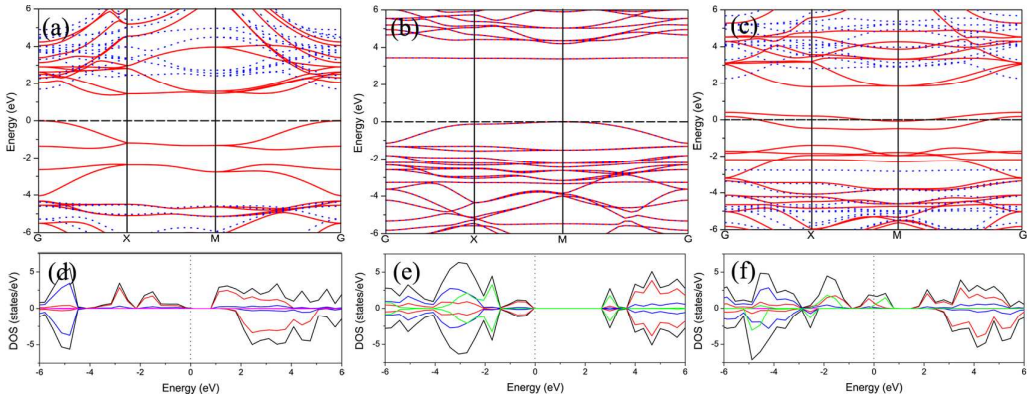

Figure 5 *The band structures of the (a) monolayer S-VO_2-2H, (b) monolayer S-VO_2-2F and*

(c) monolayer S-VO_2-HF. The corresponding DOS of the (d) monolayer S-VO_2-2H, (e) monolayer S-VO_2-2F and (f) monolayer S-VO_2-HF. The red solid lines and blue dashed lines in the band structures images represent the spin up bands and spin down bands, respectively. The black, red, blue, purple and green lines in the DOS images represent the total DOS, the partial DOS of V, O, H and F atoms, respectively.

To further tune the electronic and magnetic properties by surface modification, the fully-fluorinated monolayer S-VO_2 (S-VO_2-2F) and half-fluorinated monolayer S-VO_2 (S-VO_2-HF) need to be examined. The detailed informations of the band gap and magnetic moment distribution are also listed in Table 2. Interestingly, the coverages of fluorine also affect the electronic structure of the fluorinated monolayer S-VO_2. The ground state of the monolayer S-VO_2-2F is AFM, whereas the monolayer S-VO_2-HF prefers FM ground state. The band structure and DOS of the monolayer S-VO_2-2F (Figure 5 (b) and Figure 5 (e)) suggest that the monolayer S-VO_2-2F is also a direct band gap semiconductor at the M point with AFM coupling. The band gap of the monolayer S-VO_2-2F is 3.39 eV, which is smaller than that of the pristine monolayer S-VO_2. Strikingly, the electronic structure of the monolayer S-VO_2-HF shows that only the spin-up bands cross the Fermi level but the spin-down channels do not (see Figure 5 (c) and 5 (f)), which indicate that the monolayer S-VO_2-HF becomes half-metallic[45, 46]. The main feature of half-metallic materials is its high spin polarization up to 100%. This fascinating half-metallic magnetism, found in the monolayer S-VO_2-HF, enables the 2D monolayer to be spin-filtering device.

Finally, the origin of magnetic moment on the modified monolayer S-VO_2 is examined by the distribution of the spin density. As shown in Figure 6 (a), it is clear that the spin densities of the monolayer S-VO_2-2H are mainly localized on the V atoms with FM coupling. For the monolayer S-VO_2-2F, most of the spin densities are localized on the V and F atoms (see Figure 6 (b)). However, the AFM coupling between the top half and the bottom half results in that the monolayer S-VO_2-2F does not exhibit macro magnetism. As shown in Figure 6 (c), the spin-up densities are localized on the V atoms with FM coupling, while the spin down densities are localized on the F and the nearby O atoms. The monolayer S-VO_2-HF still exhibits macro magnetism due to the spin up densities obviously larger than the spin down densities.

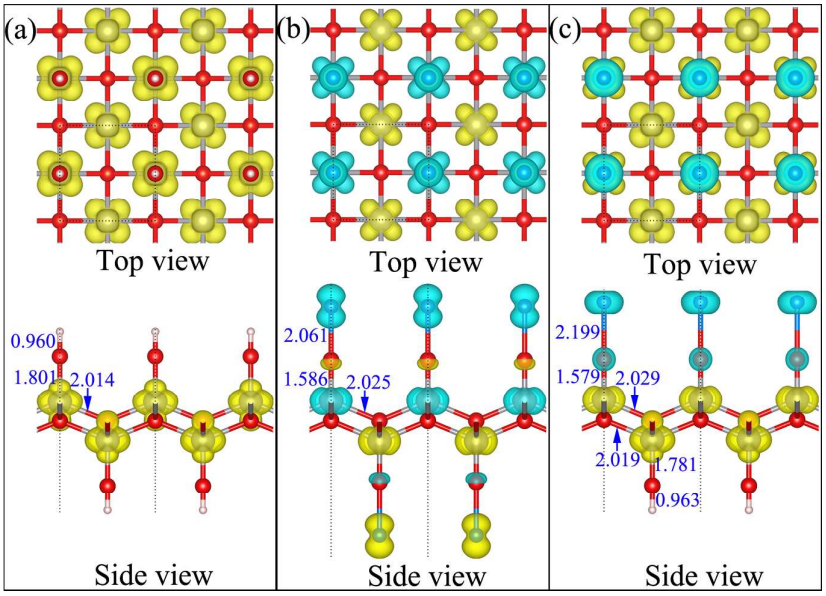

Figure 6 *The spin density distributions of the (a) monolayer S-VO_2-2H, (b) monolayer S-VO_2-2F and (c) monolayer S-VO_2-HF. The red, grey, pink and blue balls represent O, V, H, and F atoms, respectively. The yellow and green isosurfaces correspond to the spin up and spin down density, respectively.*

4. Conclusion

Based on first-principle calculations, we demonstrate that the monolayer S-VO_2 owns versatile electronic properties, which provide a flexible platform to manipulate the magnetic properties. The phonon dispersion spectrums show that the monolayer S-VO_2 is the thermodynamically stable structure. Although the pristine S-VO_2 does not own no macro magnetism with AFM coupling between two nearest V atoms, the monolayer S-VO_2 can become FM under a biaxial compressive strain reaches 8%. Furthermore, the FM ground state of the monolayer S-VO_2 with the large magnetic moments (about 4 μ_B per cell) can also be achieved by the surface hydrogenate. More interestingly, the monolayer S-VO_2-HF exhibits unusual HM properties with the spin up states exhibit metallic properties while the spin down states are semiconductor, the properties can be tuned from nonmagnetic semiconductor to magnetic semiconductor and to half-metal by adjusting the structure from S-VO_2-2F to S-VO_2-2H and to S-VO_2-HF. The tunable magnetic properties of the monolayer S-VO_2 open a new door to design the spintronic devices in the pristine 2D nanostructures.

Acknowledgments

This work was supported by the National Natural Science Foundation of China (No. 51222212, 11447011), the MOST of China (973 Project, Grant NO. 2011CB922200), the Hunan Provincial Natural Science Foundation of China (No. 2015JJ6013), the Science Foundation of Hengyang Normal University (No. 13B41), the Hunan Provincial Applied Basic Research Base of Optoelectronic Information

Technology (No. GDXX002), and the Construct Program for Key Disciplines in Hunan Province.

References

1. K. S. Novoselov, D. Jiang, F. Schedin, T. J. Booth, V. V. Khotkevich, S. V. Morozov and A. K. Geim, *PNAS*, 2005, **102**, 10451-10453.
2. M. Xu, T. Liang, M. Shi and H. Chen, *Chem. Rev.*, 2013, **113**, 3766-3798.
3. A. Du, Z. Zhu and S. C. Smith, *J. Am. Chem. Soc.*, 2010, **132**, 2876-2877.
4. S. Wangmo, R. Song, L. Wang, W. Jin, D. Ding, Z. Wang and R.-Q. Zhang, *J. Mater. Chem.*, 2012, **22**, 23380-23386.
5. L.-C. Xu, R.-Z. Wang, M.-S. Miao, X.-L. Wei, Y.-P. Chen, H. Yan, W.-M. Lau, L.-M. Liu and Y.-M. Ma, *Nanoscale*, 2014, **6**, 1113-1118.
6. F. Li, J. Gao, J. Zhang, F. Xu, J. Zhao and L. Sun, *J. Mater. Chem. A*, 2013, **1**, 8016-8022.
7. S. A. Wolf, D. D. Awschalom, R. A. Buhrman, J. M. Daughton, S. von Molnár, M. L. Roukes, A. Y. Chtchelkanova and D. M. Treger, *Science*, 2001, **294**, 1488-1495.
8. P. Grünberg, R. Schreiber, Y. Pang, M. B. Brodsky and H. Sowers, *Phys. Rev. Lett.*, 1986, **57**, 2442-2445.
9. M. N. Baibich, J. M. Broto, A. Fert, F. N. Van Dau, F. Petroff, P. Etienne, G. Creuzet, A. Friederich and J. Chazelas, *Phys. Rev. Lett.*, 1988, **61**, 2472-2475.
10. Y. Ma, Y. Dai, M. Guo, C. Niu, Y. Zhu and B. Huang, *ACS NANO*, 2012, **6**, 1695-1701.
11. H. Zhang, L.-M. Liu and W.-M. Lau, *J. Mater. Chem. A*, 2013, **1**, 10821.
12. M. Kan, J. Zhou, Q. Sun, Y. Kawazoe and P. Jena, *J. Phys. Chem. Lett.*, 2013, **4**, 3382-3386.
13. M. Kan, S. Adhikari and Q. Sun, *Phys. Chem. Chem. Phys.*, 2014, **16**, 4990.
14. D. Gao, Q. Xue, X. Mao, W. Wang, Q. Xu and D. Xue, *J. Mater. Chem. C*, 2013, **1**, 5909.
15. C. Ataca, H. Şahin and S. Ciraci, *J. Phys. Chem. C*, 2012, **116**, 8983-8999.
16. N. V. Podberezskaya, S. A. Magarill, N. V. Pervukhina and S. V. Borisov, *J. Struct. Chem.*, 2001, **42**, 654-681.
17. A. Cavalleri, C. Tóth, C. Siders, J. Squier, F. Ráksi, P. Forget and J. Kieffer, *Phys. Rev. Lett.*, 2001, **87**, 237401.
18. M. Haverkort, Z. Hu, A. Tanaka, W. Reichelt, S. Streltsov, M. Korotin, V. Anisimov, H. Hsieh, H. J. Lin, C. Chen, D. Khomskii and L. Tjeng, *Phys. Rev. Lett.*, 2005, **95**, 196404.
19. M. M. Qazilbash, M. Brehm, B. G. Chae, P. C. Ho, G. O. Andreev, B. J. Kim, S. J. Yun, A. V. Balatsky, M. B. Maple, F. Keilmann, H. T. Kim and D. N. Basov, *Science*, 2007, **318**, 1750-1753.
20. S. Zhang, B. Shang, J. Yang, W. Yan, S. Wei and Y. Xie, *Phys. Chem. Chem. Phys.*, 2011, **13**, 15873.
21. C. Wu, F. Feng and Y. Xie, *Chem. Soc. Rev.*, 2013, **42**, 5157.
22. T. A. Chirayil, P. Y. Zavalij and M. S. Whittingham, *J. Electrochem. Soc.*, 1996, **143**, L193-L195.
23. T. Chirayil, P. Zavalij and M. S. Whittingham, *Solid State Ionics*, 1996, **84**, 163-168.
24. N. A. Chernova, M. Roppolo, A. C. Dillon and M. S. Whittingham, *J. Mater. Chem.*, 2009, **19**, 2526-2552.
25. G. Kresse and J. Furthmüller, *Phys. Rev. B*, 1996, **54**, 11169-11186.
26. G. Kresse and J. Furthmüller, *Comput. Mater. Sci.*, 1996, **6**, 15-50.
27. G. Kresse and D. Joubert, *Phys. Rev. B*, 1999, **59**, 1758-1775.
28. J. P. Perdew, K. Burke and M. Ernzerhof, *Phys. Rev. Lett.*, 1996, **77**, 3865-3868.

29. J. Heyd, G. E. Scuseria and M. Ernzerhof, *J. Chem. Phys.*, 2003, **118**, 8207-8215.
30. J. Heyd, G. E. Scuseria and M. Ernzerhof, *J. Chem. Phys.*, 2006, **124**, 219906.
31. A. Togo, F. Oba and I. Tanaka, *Phys. Rev. B*, 2008, **78**, 134106.
32. K. Parlinski, Z. Q. Li and Y. Kawazoe, *Phys. Rev. Lett.*, 1997, **78**, 4063-4066.
33. M. Hybertsen and S. Louie, *Phys. Rev. Lett.*, 1985, **55**, 1418-1421.
34. M. Hybertsen and S. Louie, *Phys. Rev. B*, 1986, **34**, 5390-5413.
35. G. M. Dalpian, S.-H. Wei, X. G. Gong, A. J. R. da Silva and A. Fazzio, *Solid State Commun.*, 2006, **138**, 353-358.
36. Y. Zhou, Z. Wang, P. Yang, X. Zu, L. Yang, X. Sun and F. Gao, *ACS NANO*, 2012, **6**, 9727-9736.
37. H. Guo, N. Lu, L. Wang, X. Wu and X. C. Zeng, *J. Phys. Chem. C*, 2014, **118**, 7242-7249.
38. O. Frank, G. Tsoukleri, J. Parthenios, K. Papagelis, I. Riaz, R. Jalil, K. S. Novoselov and C. Galiotis, *ACS Nano*, 2010, **4**, 3131-3138.
39. R. J. Young, L. Gong, I. A. Kinloch, I. Riaz, R. Jalil and K. S. Novoselov, *ACS Nano*, 2011, **5**, 3079-3084.
40. D. W. Boukhvalov, M. I. Katsnelson and A. I. Lichtenstein, *Phys. Rev. B*, 2008, **77**, 035427.
41. J. Zhou, M. M. Wu, X. Zhou and Q. Sun, *Appl. Phys. Lett.*, 2009, **95**, 103108.
42. H.-J. Kim and J.-H. Cho, *Phys. Rev. B*, 2013, **87**, 174435.
43. J. Philip, A. Punnoose, B. I. Kim, K. M. Reddy, S. Layne, J. O. Holmes, B. Satpati, P. R. LeClair, T. S. Santos and J. S. Moodera, *Nat. Mater.*, 2006, **5**, 298-304.
44. Z.-K. Tang, L.-M. Tang, D. Wang, L.-L. Wang and K.-Q. Chen, *EPL*, 2012, **97**, 57006.
45. J. M. D. Coey and S. Sanvito, *J. Phys. D: App. Phys.*, 2004, **37**, 988.
46. M. I. Katsnelson, V. Y. Irkhin, L. Chioncel, A. I. Lichtenstein and R. A. de Groot, *Rev. Mod. Phys.*, 2008, **80**, 315-378.